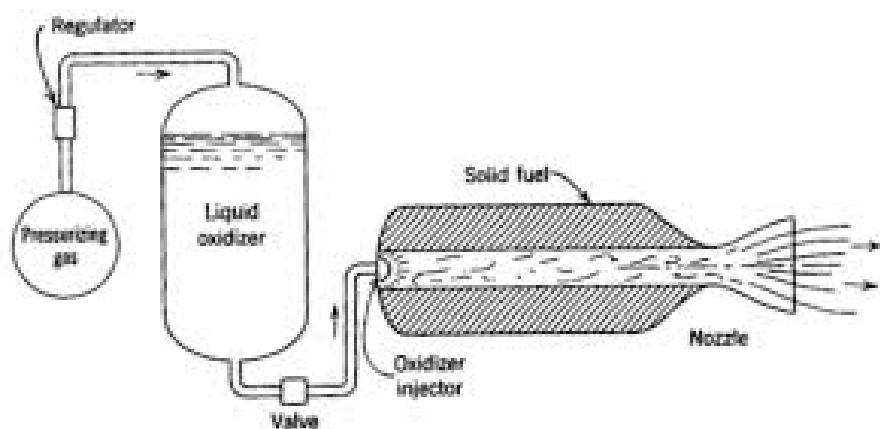


ENGINEERING MODELING PROJECT - Q4 -2016

PRESSURE MEASUREMENTS IN HYBRID ROCKET

AARHUS UNIVERSITY
DEPARTMENT OF ENGINEERING



CASPER GRØNNE CHRISTENSEN

FABIAN TOSCHÉ

NICKLAS RAFN

TIM DREBES

JUNE 3, 2016

This page is intentionally left blank

Title page

Title Pressure measurements in a hybrid rocket
Course Engineering Modeling project
Period April – June 2016 (Q4)
Group 6

Supervisor Gorm Bruun Andresen
gmb@eng.au.dk

Group Members Casper Grønne Christensen _____
20115372@post.au.dk _____
Signature

Date

Fabian Tosché _____
201503809@post.au.dk _____
Signature

Date

Nicklas Rafn _____
201270206@post.au.dk _____
Signature

Date

Tim Drebes _____
201503808@post.au.dk _____
Signature

Date

Contents

Title page	i
Contents	ii
0 Introduction	1
0.1 Thesis Statement	1
1 Theory	2
1.1 Hybrid Rocket	2
1.2 Rocket Propulsion	4
1.3 Nozzle Theory	5
1.4 Thrust of the present rocket	8
1.5 Efficiency	9
1.6 Combustion Instability	10
2 Experimental Setup	11
2.1 Watertest	11
2.2 Safety	12
2.3 Data acquisition	13
2.4 Sensors	14
2.5 Sensor Calibration	16
3 Data Analysis	18
3.1 The Data	18
3.2 Methods of Analysis	24
3.3 Results	26
4 Discussion and Conclusion	35
4.1 Discussion	35
4.2 Conclusion	35
Bibliography	36

Chapter 0

Introduction

This project concerns the pressure distribution of gases and density wave propagation speed inside the combustion-, precombustion- and fuel-chamber of a simple hybrid rocket.

0.1 Thesis Statement

Implication of three different types of pressure sensors, investigates the following.
Sensors:

- What is the frequency spectrum at which the pressure and mechanical system oscillates?
- What is the maximum frequency of the pressure oscillations, and hence how high quality sensor is needed, in order to capture all data without aliasing?

Travel time between pressure sensors:

- How fast does the pressure travel from one sensor to another to another and what average temperatures does this signify?
- and is the pressure sensors fast enough to measure the travel of pressure in the rocket?

Chapter 1

Theory

1.1 Hybrid Rocket

A rocket in general is called a hybrid rocket if they use a liquid and a solid as propellants, which burns as a macroscopic turbulent diffusion flame. This hybrid rocket has an attractive alternative to the conventional liquid and solid rockets. The following chapter comprises a rough introduction of the tested hybrid rocket and the advantages and disadvantages compared to a liquid or a solid rocket.

1.1.1 Build-up of tested rocket

The tested hybrid rocket consists of two main components. The liquid oxidizer, in our case hydrogen peroxide, is stored in a pressure tank out of stainless steel. The tank has a volume of three litres and operates at a pressure of 20 bar. Hydrogen peroxide is used for pressuring. From this tank the oxidizer floats into the combustion chamber where our solid propellant is kept. As solid fuel several round MDF-plates got glued together. By drilling the plates in advance spiralled holes were inserted. In this combustion chamber the liquid propellant vaporize, develops a chemical reacting boundary layer over the solid-fuel surface and occur in a boundary layer diffusion flame. The combustion gives a high pressure in the combustion chamber. The nozzle converts the high pressure and temperature, low speed in the combustion chamber into a gas at high speed but lower pressure and temperature. This is used to translate the pressure into thrust.

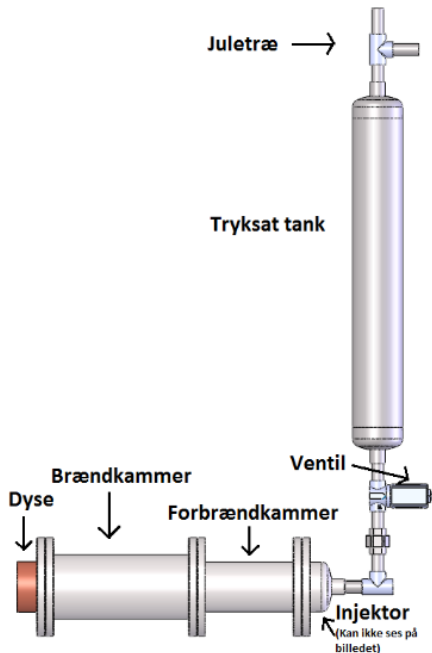


Figure 1.1: Build-up of tested hybrid rocket

1.1.2 Advantages and Disadvantages

Between a classic hybrid rocket and a fluid or solid rocket are as mentioned before significant differences which guide to some considerable advantages and disadvantages of a hybrid rocket.

Advantages

- To throttle the engine of a liquid rocket two different flow rates have to be modulated, whereas for a hybrid rocket it is only one. This leads to a simplified throttling, since the change in the oxidizer flow regulates the fuel flow rate. Hence, by switching off the liquid flow rate the engine can be shut down.
- Either liquid and solid rockets need specific propellants to get their engine work, in which the versatility of propellants for hybrid rockets is much greater. A nice side effect, compared to solids, the liquid oxidizer features much higher energy levels.
- The hybrid rocket is, compared to the others, safe since the oxidizer and the fuel are not explosive and do not have to be mixed in advance. Hence, the fuel can be manufactured, transported and handled safely.
- The burn rate of hybrid rockets is only slightly effected by **the temperature effect**. Thus, the variation of the environmental temperature has only a minor effect on the pressure in the operating chamber. Furthermore, no special design of the rocket to ensure the maximum operating pressure is needed.

- The advantages mentioned before enable to keep the costs for the hybrid rocket quite low. All the safety features and in particular the inert propellant are the main factors. The fuel production can be done in a commercial environment and does not require any safety precautions.

Disadvantages

- The opening of the port and the constant oxidizer flow-rate cause a change of the ratio of fuel rate to oxidizer flow rate with burning time which lowers the theoretical performance. However, with an accurate design the impact is marginal and the loss will be minimized to less than 1%.
- The typical low regression rate of a hybrid requires multiple ports for combustion chambers over a foot in diameter. Thereby, a adequate burning surface will be provided to meet the provided thrust.
- A lower impulse efficiency of the hybrid rocket results from the large diffusion flame. This lower degree of mixing is generally 1-2% greater than in solid or liquid rockets.

1.2 Rocket Propulsion

The thrust responsible for the propulsion of the rocket, because of changes in momentum, is given by

$$F = \frac{dm}{dt} v_2 = \dot{m} v_2 \quad (1.1)$$

where v_2 is the exit velocity for the gas and \dot{m} is the mass flow. This equation is on its own not enough to describe the total thrust of the rocket as the pressure of the atmosphere has been neglected. The final equation is therefore the following,

$$F = \dot{m} v_2 + (p_2 - p_3) A_2 \quad (1.2)$$

where p_2 is the local pressure at the exit of the rocket, p_3 is the atmospheric pressure and A_2 is the area of the rocket/gas exit. As can easily be seen, the second term of this equation has the possibility to produce negative thrust if the exit pressure is lower then atmospheric pressure. This is undesirable as it will reduce the total thrust of the rocket, therefore the nozzle is often engineer such that the exit pressure is equal to or slightly higher then the atmospheric pressure. When this is true ($p_2 = p_3$) the equation is reduced to eq: 1.1, and is know as the *optimum expansion ratio*. This equation also shows that we have a change in thrust depending on the altitude, as the atmospheric pressure changes.

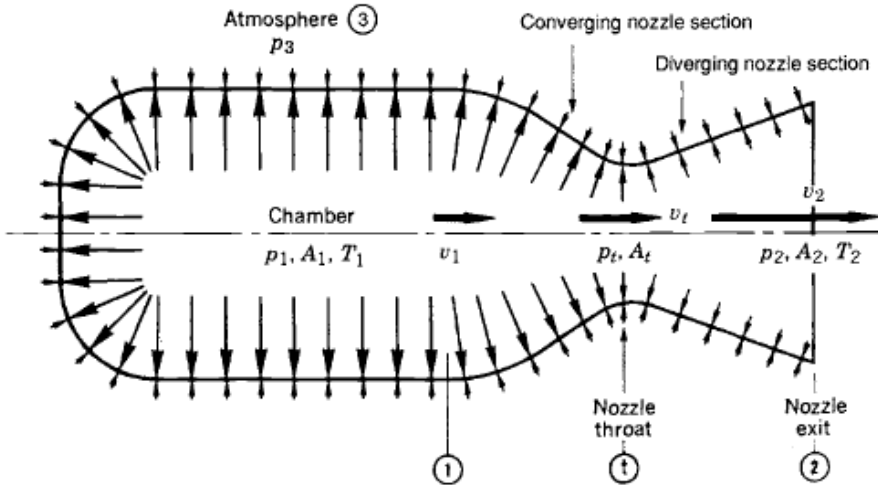


Figure 1.2: Pressure balance inside rocket

1.3 Nozzle Theory

In the present chapter the influence of the condition (pressure and temperature) inside the combustion chamber of the rocket on the thrust is outlined. These dependencies are determined based on thermodynamic equations under certain assumptions. Most important a steady flow, an adiabatic process and an ideal gas is assumed. Furthermore the friction in the nozzle can be neglected and the exhaust velocity field is presumed to be axial. The objective is to derive the components of equation 1.1. Figure 1.2 outlines the system and notation. Based on the energy equation the total Enthalpy in the combustion chamber is determined.

$$h_0 = h + \frac{v^2}{2} = \text{constant} \quad (1.3)$$

In the present set up this equation becomes

$$v_2 = \sqrt{2(h_1 - h_2) + v_1^2} \quad (1.4)$$

Assuming a stagnation inside the chamber results in

$$v_1 = 0. \quad (1.5)$$

Hence,

$$v_2 = \sqrt{2(h_1 - h_2)} \quad (1.6)$$

The assumption of a perfect caloric gas

$$h = c_p T \quad (1.7)$$

with c_p being the heat capacity at constant pressure leads to

$$v_2 = \sqrt{2c_p(T_1 - T_2)} \quad (1.8)$$

or rewritten to

$$v_2 = \sqrt{2c_p T_1 \left(1 - \frac{T_2}{T_1}\right)}. \quad (1.9)$$

Consider an isentropic flow gives the following relation:

$$\frac{T_2}{T_1} = \left(\frac{p_2}{p_1}\right)^{\frac{\kappa-1}{\kappa}}. \quad (1.10)$$

Inserting 1.10 into 1.9 results in

$$v_2 = \sqrt{2c_p T_1 \left(1 - \left(\frac{p_2}{p_1}\right)^{\frac{\kappa-1}{\kappa}}\right)}. \quad (1.11)$$

Since

$$c_p = \frac{\kappa R_s}{\kappa - 1} \quad (1.12)$$

with the adiabatic index and the heat capacity at constant volume

$$\kappa = \frac{c_p}{c_v} \quad (1.13)$$

Equation 1.11 becomes

$$v_2 = \sqrt{2 \frac{\kappa R}{\kappa - 1} T_1 \left(1 - \left(\frac{p_2}{p_1}\right)^{\frac{\kappa-1}{\kappa}}\right)}. \quad (1.14)$$

In the next step the isentropic flow relation is determined. The energy relation and the assumption of a perfect caloric gas leads to

$$T_1 = T_2 + \frac{v^2}{2c_p} \quad (1.15)$$

$$\frac{T_1}{T_2} = 1 + \frac{v^2}{2c_p T_2} = 1 + \frac{v^2}{2 \frac{\kappa R_s T_2}{\kappa - 1}}. \quad (1.16)$$

Introducing the Mach Number

$$M = \frac{v}{a} \quad (1.17)$$

and the speed of sound

$$a^2 = \kappa R_s T. \quad (1.18)$$

leads to

$$\frac{T_1}{T_2} = 1 + \frac{\kappa - 1}{2} M^2 \quad (1.19)$$

For an adiabatic process the pressure ratio is determined by

$$\frac{p_1}{p_2} = \left(\frac{T_1}{T_2} \right)^{\frac{\kappa}{\kappa-1}} \quad (1.20)$$

and hence,

$$\frac{p_1}{p_2} = \left(1 + \frac{\kappa - 1}{2} M^2 \right)^{\frac{\kappa}{\kappa-1}} \quad (1.21)$$

With the consideration of the previous derivations the mass flow rate through the nozzle can be determined. Mass conversation gives

$$\dot{m} = \rho v A \quad (1.22)$$

with the assumption of a ideal gas:

$$\rho = \frac{p}{RT} \quad (1.23)$$

and the previous defined Mach Number and speed of sound

$$\dot{m} = \frac{p}{R_s T} M \sqrt{\kappa R_s T} A \quad (1.24)$$

Rewriting for later use and introducing the notation of the actual problem results in

$$\dot{m} = \frac{p_2}{p_1} p_1 M \sqrt{\frac{\kappa}{R_s T_1}} \sqrt{\frac{T_1}{T_2}} A \quad (1.25)$$

Consider the temperature and pressure ratio, obtained in 1.10 and 1.21:

$$\dot{m} = \left(1 + \frac{\kappa - 1}{2} M^2 \right)^{-\frac{\kappa}{\kappa-1}} p_1 M \sqrt{\frac{\kappa}{R_s T_1}} \sqrt{1 + \frac{\kappa - 1}{2} M^2} A \quad (1.26)$$

Assuming $M = 1$ inside the Lavalnozzle gives

$$\dot{m} = P_1 \kappa A_t \sqrt{\frac{1}{\kappa R_s T_1} \left(\frac{2}{\kappa + 1} \right)^{\frac{\kappa+1}{\kappa-1}}} \quad (1.27)$$

with the area of the throat A_t .

General conclusions of the influence of certain parameters and conditions on the actual thrust can be drawn by the previous equations. Based on equation 1.1 it is desirable to obtain high numbers both for equation 1.14 and equation 1.27 which are influencing each other naturally. The biggest influence on the thrust is the pressure inside the combustion chamber p_1 since \dot{m} is linearly dependent and v_2 lists p_1 in the denominator which leads

in this case also to a slightly increase of the thrust (in case of an increasing pressure). The influence of the temperature inside the combustion chamber T_1 can be neglected in regard of the actual thrust, but by nature the matter constants are dependent on the temperature as well as equation 1.10 and therefore the above mentioned pressure. Especially the heat capacity ratio in equation 1.27 has a great influence on the mass flow and is dependent on the temperature in the chamber as well. The area of the outlet seems to have a huge impact on the mass flow due to equation 1.27 but it has to be considered that a small outlet of the nozzle is crucial for a high stagnation pressure. The ideal gas constants do not have an influence on the resulting thrust.

1.4 Thrust of the present rocket

In this section the actual thrust of the hybrid rocket is calculated using the equations in the previous chapters. Numbers are either obtained by the tests or reasonable assumptions. For determining the thrust the components of equation 1.1 are calculated. The mass flow is derived by equation 1.27 and equation 1.14 gives the exhaust velocity. Since the exhaust persists mostly out of carbon dioxide CO_2 and Nitrogen N_2 the other parts like water are neglected since this section aims to give a rough outline of the thrust. Therefore the chemical properties of CO_2 are used ($R_s = 189 \text{ J/KgK}$) and ($\kappa = 1.16$) Based on table 3.3.3 an assumption of a temperature $T_1 = 2000\text{K}$ inside the combustion chamber seems to be reasonable. The diameter of the injector is read out of the technical drawing and therefore the outlet of the nozzle is determined. The average pressure inside the chamber ($p_1 = 17\text{bar}$) was measured during the tests (see Chapter 3). Inserting these values into equation 1.27 gives:

$$\dot{m} = 17 \cdot 10^5 \frac{N}{m^2} \cdot 1.16 \cdot (21.3m \cdot 10^{-3})^2 \frac{\pi}{4} \sqrt{\frac{1}{1.16 \cdot 189 \frac{J}{kgK} \cdot 2000K}} \left(\frac{2}{1.16 + 1} \right)^{\frac{1.16+1}{1.16-1}} \quad (1.28)$$

Resulting in a mass flow through the nozzle of $\dot{m} = 0.61\text{kg/s}$ With $p_2 = 0.9\text{bar}$ The exhaust velocity is obtained by:

$$v_2 = \sqrt{2 \cdot \frac{1.16 \cdot 189 \frac{J}{kgK}}{1.16 - 1} \cdot 2000K \cdot \left(1 - \left(\frac{0.9\text{bar}}{17\text{bar}} \right)^{\frac{1.16-1}{1.16}} \right)}. \quad (1.29)$$

The outcome is $v_2 = 1351\text{m/s}$, leading into a resulting thrust of

$$F = 0.61 \frac{kg}{s} \cdot 1351 \frac{m}{s} = 824.39N \quad (1.30)$$

Conducting the same calculations with the other main component of the exhaust gas which is nitrogen ($R_s = 297 \text{ J/kgK}$) and ($\kappa = 1.3$) leads to a similar range of the trust ($\dot{m} = 0.524 \frac{kg}{s} \cdot 1592 \frac{m}{s} = 834.3N$). This value slightly overshoots the test results. But in consideration of the made assumptions and in awareness that the theoretical derivation

of the thrust represents a perfect combustion which can not be accomplished in the real testing, the value is reasonable. Furthermore the pressure inside the combustion chamber varies during the actual combustion.

1.5 Efficiency

In the present section the efficiency of the rocket combustion is briefly described. The efficiency represents the actual conversation rate of the energy inside the combustion chamber or in general of the energy input (H_2O_2 and MDF plates) to actual thrust. The Carnot's theorem gives the maximum efficiency of a heat engine and is based on the second law of thermodynamics. This theorem only takes the maximum (T_{max}) and minimum (T_{min}) temperature in a process into account and neglects for example losses due to compression:

$$\eta_{carnot} = 1 - \frac{T_{min}}{T_{max}} \quad (1.31)$$

Since no data set regarding the temperature in the exhaust outside of the nozzle exists an actual number for η_{carnot} cannot be determined to the current status. T_{max} is equal to the above derived T_1 inside the combustion chamber. Based on assumption the temperature $T_t = T_{min}$ inside the throat can be obtained and therefore η_{carnot} derived. The density ρ of the exhaust gas is assumed to be constant (incompressible flow). Hence,

$$\rho = \frac{\dot{m}}{v_2 \cdot A_t} \quad (1.32)$$

According to Bernoulli the pressure p_t inside the throat can be derived by

$$p_t = p_1 - \rho \cdot \frac{v_2^2}{2} \quad (1.33)$$

Based on the following equation the temperature inside the throat can be calculated:

$$T_t = \frac{1}{\kappa R_s} \left(\frac{2}{\kappa + 1} \right)^{\frac{\kappa+1}{\kappa-1}} \left(\frac{\dot{m}}{p_t \kappa A_t} \right)^{-2} \quad (1.34)$$

For the actual rocket, the density of the exhaust (assume: Nitrogen) is:

$$\rho = \frac{0.53 \frac{kg}{s}}{1592 \frac{m}{s} \cdot (21.3 \cdot 10^{-3} m)^2 \cdot \frac{\pi}{4}} = 0.935 \frac{kg}{m^3} \quad (1.35)$$

Therefore the pressure in the throat equates to:

$$p_t = 17bar - 0.935 \frac{kg}{m^3} \cdot \frac{(1592 \frac{m}{s})^2}{2} = 5.2bar \quad (1.36)$$

Eventually the temperature in the nozzle is derived by

$$T_t = \frac{1}{1.3 \cdot 297 \frac{J}{kgK}} \left(\frac{2}{1.3 + 1} \right)^{\frac{1.3+1}{1.3-1}} \left(\frac{0.524 \frac{kg}{s}}{5.2bar \cdot 1.3 \cdot (21.3 \cdot 10^{-3} m)^2 \cdot \frac{\pi}{4}} \right)^{-2} = 188K \quad (1.37)$$

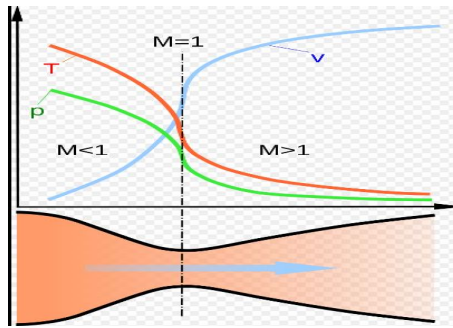


Figure 1.3: Relations in a Laval nozzle

This temperature results in a Carnot efficiency of

$$\eta_{carnot} = 1 - \frac{188K}{2000K} = 90.6\% \quad (1.38)$$

Taking all the assumptions into account and the awareness of the Carnot-process being the maximum efficiency of a heat engine this number seems to reasonable. Furthermore it is assumed that the velocity at point 2 (exit) is constant and equal to the velocity at the throat. This assumptions led to a higher outcome of p_t and therefore to a lower T_t which results in a increased η_{carnot} . The relation between pressure, temperature and velocity in a Lavalnozzle is shown in figure 1.3.

1.6 Combustion Instability

Instability of a rocket motor comes from pressure oscillations that travels through the motor. We can separate these oscillation into three categories high, medium and low frequencies

1.6.1 Medium and high frequencies

these frequencies comes from the acoustic properties of the chamber and therefore responds to the longitudinal modes of sound waves. Where the high frequencies relates to the overtones (the high modes) of the chamber.

1.6.2 Low frequencies

There are several mechanisms that gives rise to low frequency instabilities, where one of the main reasons is Chuffing.

Chuffing

Chuffing instabilities comes from the break off and creation of char on the solid fuel. The repeating behavior between the build up and removal of the char layer is what create these oscillation.

Chapter 2

Experimental Setup

In the present chapter the set-up of the experiments which were executed at Raketmadsens Rumlaboratorium in Copenhagen is outlined. This includes the data acquisition, the test procedure and safety requirements. The location of the test was chosen because it satisfies all safety requirements and on the other hand because of having the required fuel (hydrogen peroxide) available. Furthermore, the experience of Madsen could be taken into account as well.

2.1 Watertest

Before starting on the actual tests with hydrogen peroxide the rocket or more precisely the pressure tank was filled with common water and eventually pressurized. These tests were executed for the sake of getting an idea of the spray pattern of the injector, which was designed new recently and for ensuring the cleanliness of the apparatus regarding remaining chemicals or other particles. The reason for redesigning the injector was the aiming for a more optimal solution which means the propellant would be sprayed into two beams towards cross each other and therefore obtaining a more complete atomization. For the water tests the main- and precombustion chamber were removed (figure 2.1). Another reason for the tests without propellant is the checking on the proper acquisition of the sensor data. It is highly necessary that at the actual testing the measurement equipment works proper.



Figure 2.1: Watertest

2.2 Safety

Due to the huge energy release rate during the actual tests of the rocket safety needs to be taken into consideration. The whole procedure takes three different safety concerns into account. Those are first of all the handling of the hydrogen peroxide. Hydrogen peroxide needs to be handled with care since it is highly flammable and explosive which is naturally the character of a propellant. Therefore experiences is also required as well as the appropriate safety equipment. Furthermore the nitrogen which is put under a lot of high pressure needs to be handled with care. Eventually, failure during the different stages of the actual combustion e.g. due to material fatigue or mistakes in the preparation and assembly needs to be considered, a high number of sandbags were used as an additional safety measure (see figure 2.2) and protection shields (here the submarine and the metal shield). Furthermore a certain safety distance needs to be considered. The nature of hydrogen peroxide requires a fast access to running water for dilution in case of skin contact and for cleaning the components of the rocket after the test runs. The nitrogen is used for pressurizing the pressure tank and is therefore stored in a suitable high-pressure bottle in Raketauditorium. This an important point since the pressure bottle must be insulated against every potential damages during the tests. Rocket or material failure must be regarded as well, leading to a requirement of dozen sandbags on and besides the rocket. The sandbags allow a decreasing of the safety distance to approximately 100 m (still in addition to a metal shield). Ignition and observation of the environment right before the ignition were executed in and on the submarine Nautilus which is designed with steel plates with thickness of 15 mm and therefore satisfies all safety concerns.



Figure 2.2: Setup

2.3 Data acquisition

In this section the setup of the measuring equipment and the method of data logging are described.

On various points at the rocket the data is logged (see 2.4). For data logging, it is desired to measure the various points on the rocket. The collection Data from these points to a computer was made by measuring equipment which was connected to a DAQ from National Instruments with a corresponding NI 9219 analog input module. These are required for the subsequent data processing and calculations of the rocket. The data was communicated to a computer standing behind the rocket test stand. Due to the highly safety requirements this computer was operated via a remote control inside the submarine. The sensor data is transferred into a Labview programme. In the following figure 2.3 the programme is outlined.

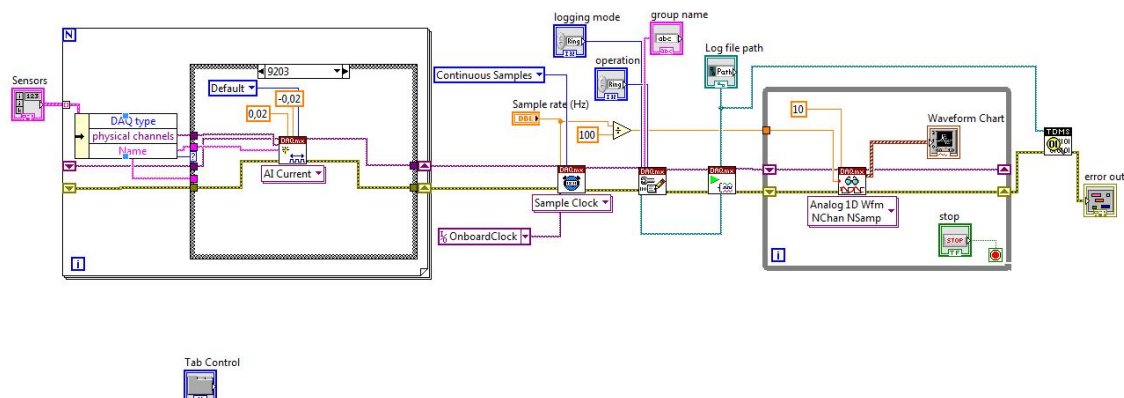


Figure 2.3: Labview programme

2.4 Sensors

By tracking the pressure pulses as they propagate within the chamber, three different kind of sensors were used. According to their data sheets they differ in accuracy and measurement speed. It should be shown which sensor fits the needs the best. Is it necessary to use the most accurate and following most expensive one or is a cheaper one still sufficient? The sensor configuration can be seen in figure 2.4.

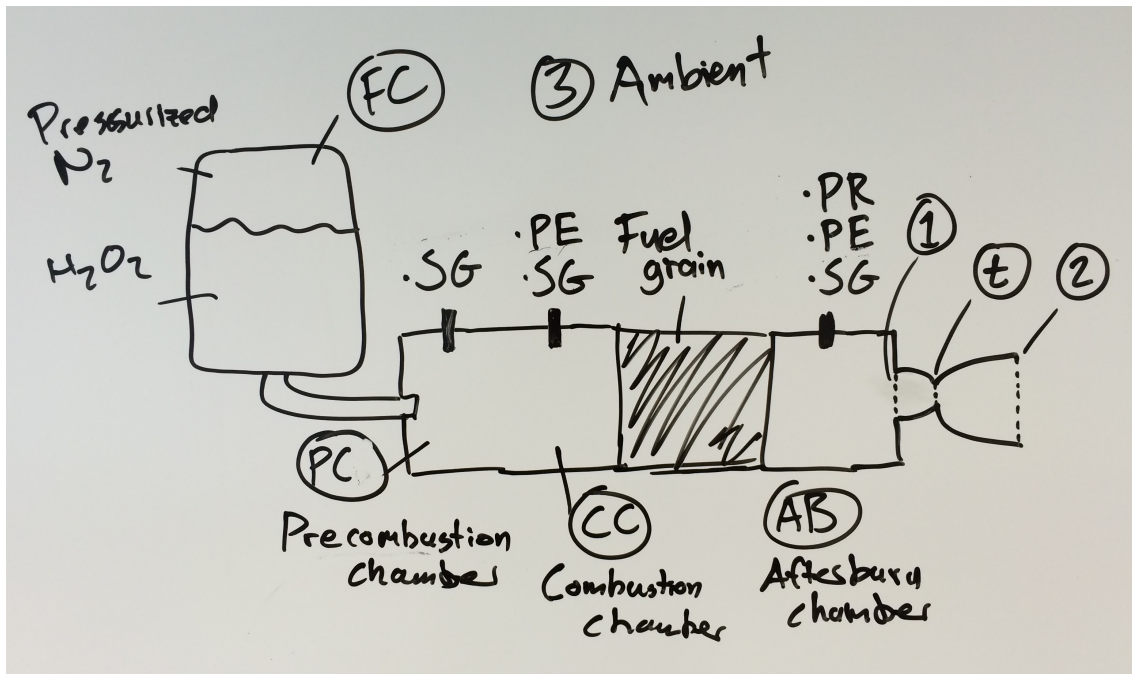


Figure 2.4: The sensor placements on the rocket

2.4.1 Strain gauge pressure sensor (SG)

This standard pressure transmitter from Danfoss is designed for the use in almost all industrial applications even in harsh environmental conditions and is one of the fundamental sensing elements. Ranges from 0 up to 600 bar can be measured and the output signal is in a range of 0 to 20 mA. If a change in pressure arises during the test a diaphragm in the sensor will be deflected. Following a corresponding change in resistance is induced on the strain gauge which can be measured. Some of the advantages are the remarkable robust construction and the excellent vibration stability. Furthermore, all strict industrial requirements are fulfilled by the high degree of electromagnetic compatibility /-interference protection of the transmitter.

2.4.2 Piezoelectric pressure sensor (PE)

The piezoelectric pressure sensor from Kistler is made for continuous cylinder pressure measurements for low and medium speed engines. The sensor operates with an out-put signal between 4 – 20 mA and a measuring range from 0 to 250 bar. The piezoelectric

pressure sensor is equipped with quartz as sensing material and uses the piezoelectric effect to measure pressure changes. This effect is a reversible process which is the interaction between a mechanical and an electrical state in crystalline materials. By deforming the quartz by pressure an electric charge occurs. This so called piezoelectricity can be measured and yields the output. Important to know is that this is a dynamic effect which means that this sensor can be used only for varying pressures. A perfect long term stability is guaranteed by the robust design. In addition, the quartz-measuring element creates an extremely accurate and repeatable output signal over the whole lifetime. The sensor features a very good thermodynamic behaviour.

2.4.3 Piezoresistive pressure sensor (PR)

The piezoresistive pressure sensor from Kistler is a versatile high performance sensor originally invented for the research and development sector in automotive and aerospace. It operates within a pressure range of -1 to 350 bar and has an exceeding fast response time. In this sensor the piezoresistive effect is used to measure the pressure differences. Semiconductors, in our case silicon, are used that change their electrical resistivity when they are compressed or strained. These materials are connected to devices (e.g. Wheatstone bridge) for detecting small differences in electrical resistance. By using the technology of a silicon sensing element high performances of stability and repeatability can be maintained. These are one of the most important things for engineering tests.

2.4.4 Comparison of sensors

Quantity	Strain gauge	Piezoelectric	Piezoresistive
Pressure range	0-600 bar	0-250 bar	-1-350 bar
Frequency	250 Hz	10 kHz	2 kHz
Sensitivity	0,2% FS	0,05% FS	0,05% FS
Accuracy	0,3% FS	0,1% FS	0,05% FS
Non-linearity	0,2% FS	0,5% FS	0,1% FS

Table 2.1: Comparison of sensors

Explanation of terminology used in the table:

- Pressure range: The range of the sensor is the maximum and minimum values of applied parameter that can be measured.
- Sensitivity: The sensitivity of the sensor is defined as the minimum input of physical parameter that will create a detectable output change.
- Accuracy: The accuracy of the sensor is the maximum difference that will exist between the actual value (which must be measured by a primary or good secondary standard) and the indicated value at the output of the sensor.

- Non-linearity: The linearity of the transducer is an expression of the extent to which the actual measured curve of a sensor departs from the ideal curve.

2.5 Sensor Calibration

The output signal from the sensors (pressure transmitter, piezoelectric and piezoresistive) is current, voltage and charge. The sensitivity is not given by the manufacturer, and a calibration process have to be made. This is done with a calibrator that is basically just a more accurate sensor and a pressure chamber that can vary the pressure. The calibration setup is shown on figure 2.5.



Figure 2.5: Pressure calibrator

For each sensor, circa six measurements are made, and the data is fitted with linear regression. The results from the calibration process can be seen in Table 2.2. It shows from the R-squares that the calibration process has a very high precision and the sensors can be trusted. The conversion from electrical signal to pressure is implemented in the data analysis in chapter 2.3.

Table 2.2: Sensitivity of sensors

Sensor	Conversion	R-square
Danfoss ZERO	$I = 0.397 \text{ mA/barG } p + 4.01 \text{ mA}$	1.0000
Danfoss ONE	$I = 0.398 \text{ mA/barG } p + 3.98 \text{ mA}$	1.0000
Danfoss TWO	$I = 0.398 \text{ mA/barG } p + 3.97 \text{ mA}$	1.0000
Danfoss THREE	$I = 0.416 \text{ mA/barG } p + 3.81 \text{ mA}$	0.9962
Kistler PZR	$U = 0.266 \text{ V/barG } p + 60.6 \text{ mV}$	0.9984
Kistler PZE	$Q = 21.4 \text{ pC/bar}$	N/A

Chapter 3

Data Analysis

3.1 The Data

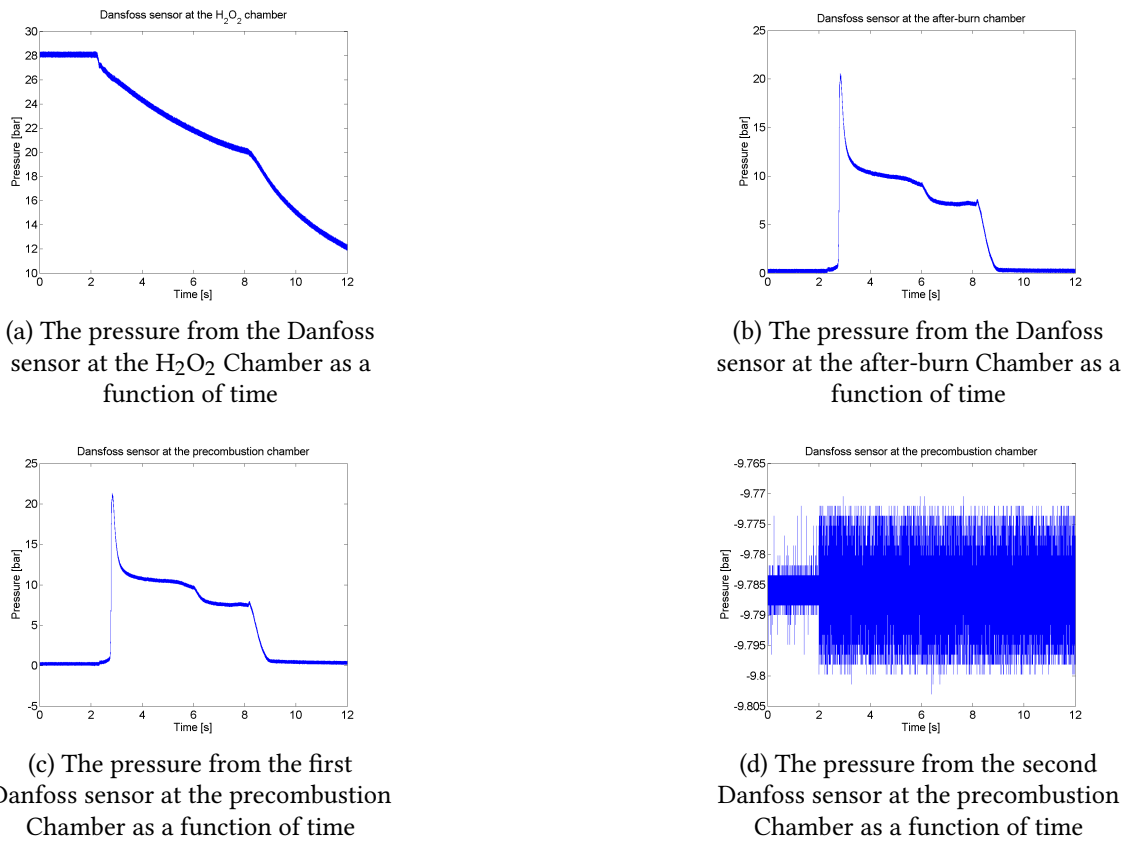
In this section the data acquired doing the experiments will be presented.

3.1.1 Burn 1

During the first burn a leak at the rocket occurred. Thus, there are no meaningful datas which could have been analysed.

3.1.2 Burn 2

For the second burn of the rocket the previous problems could be solved and the engine without any problems. However, the second Danfoss sensor at the precombustion chamber was not connected properly to the data acquisition system so the received data is only noise. The Pressure of the of the H₂O₂ chamber falls nicely linearly, and the data from the precombustion and after-burn chamber is similar in both the PE and Danfoss sensors. The data from the PE-sensors have at the end of the run drifted a bit as can be seen by the slight raise it have from zero bar.



(a) The pressure from the Danfoss sensor at the H₂O₂ Chamber as a function of time

(b) The pressure from the Danfoss sensor at the after-burn Chamber as a function of time

(c) The pressure from the first Danfoss sensor at the precombustion Chamber as a function of time

(d) The pressure from the second Danfoss sensor at the precombustion Chamber as a function of time

Figure 3.1: The Data from the four Danfoss sensors at different location on the Hybrid-rocket

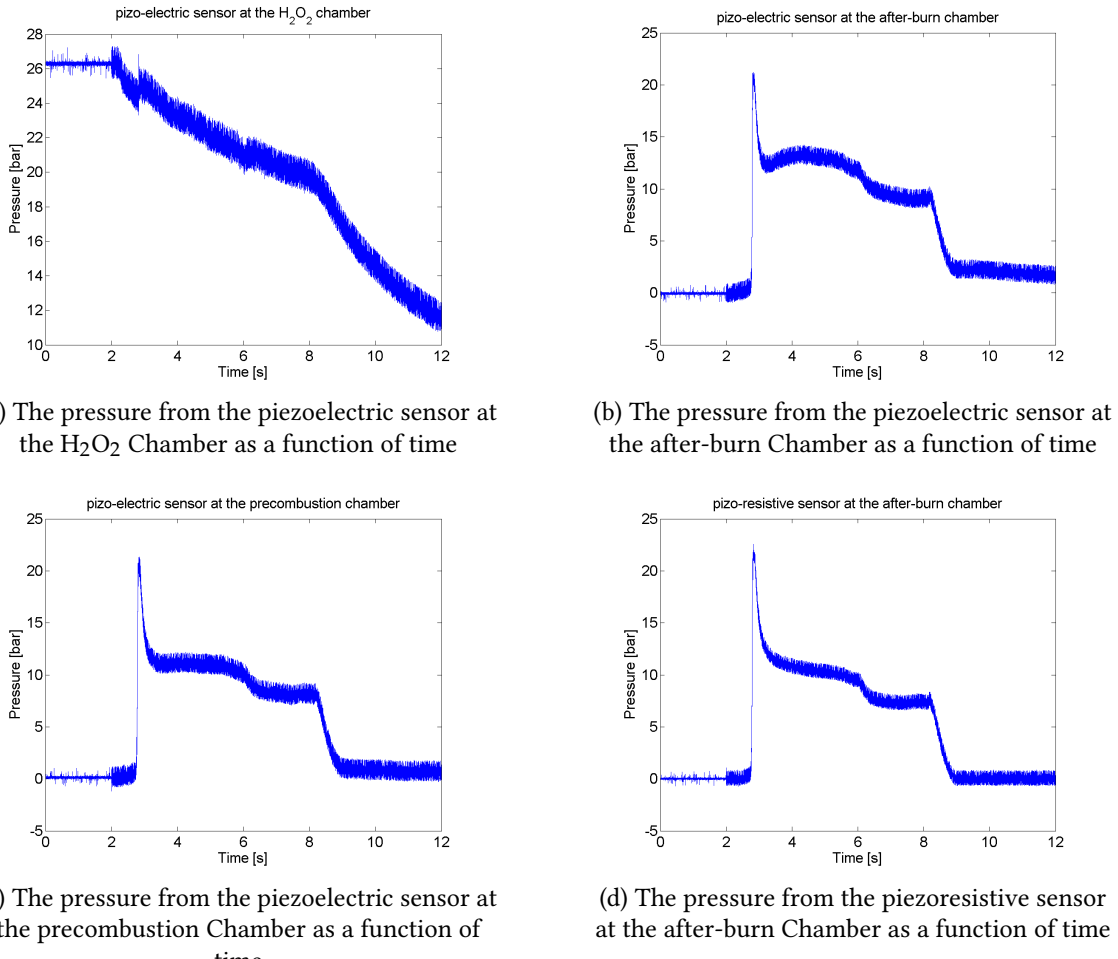
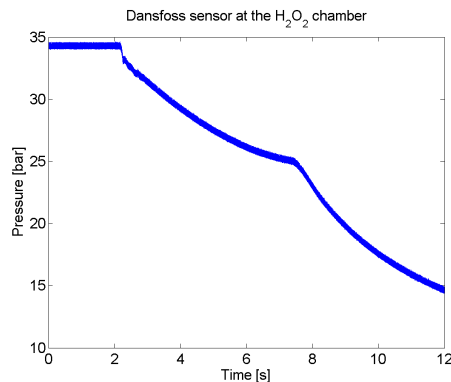


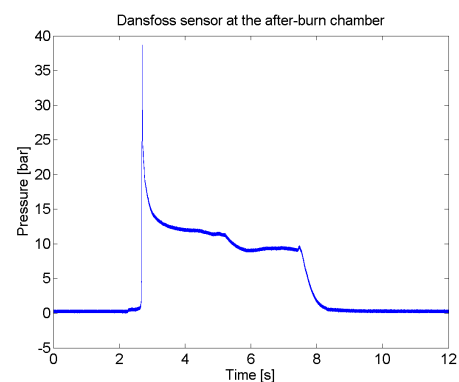
Figure 3.2: The Data from three piezoelectric and one piezoresistive sensor at different location on the hybrid rocket

3.1.3 Burn 3

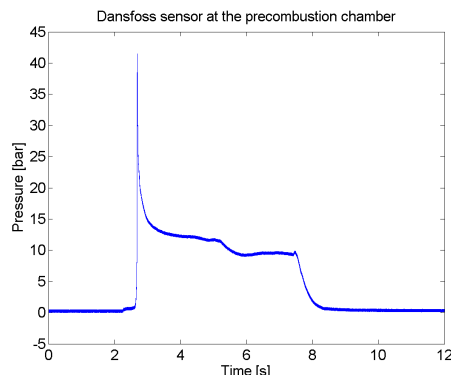
For the Third burn the engine functioned without any problems. However, the second Danfoss sensor at the precombustion chamber was not connected properly to the data acquisition system so the received data is only noise. The Pressure of the H₂O₂ chamber falls nicely linearly, and the data from the precombustion and after-burn chamber is similar in both the PE, PR and Danfoss sensors. The data from the PE-sensors have at the end of the run drifted a bit as can be seen by the slight raise it have from zero bar.



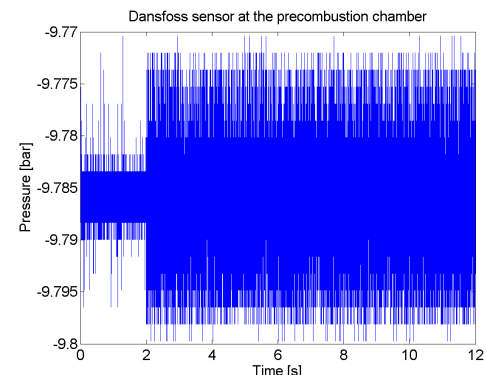
(a) The pressure from the Danfoss sensor at the H₂O₂ Chamber as a function of time



(b) The pressure from the Danfoss sensor at the after-burn Chamber as a function of time

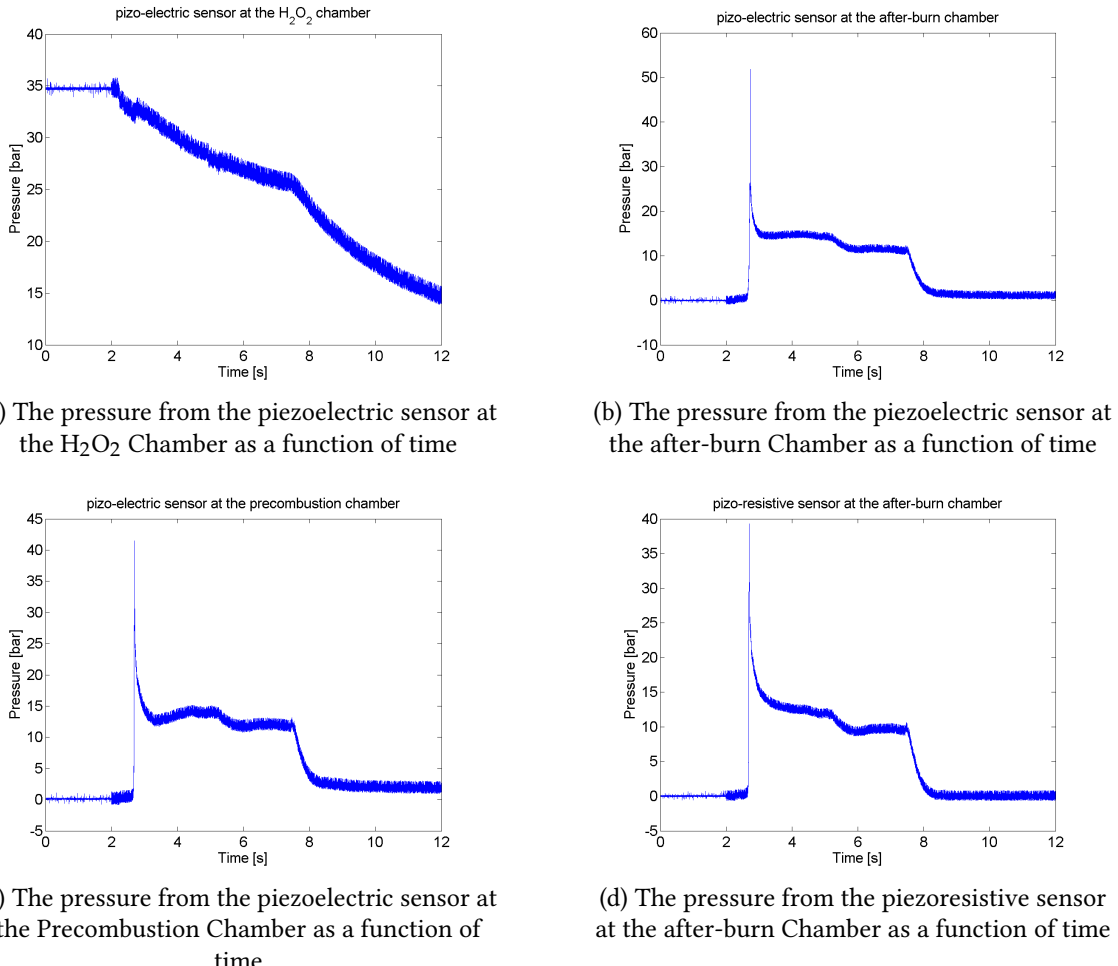


(c) The first pressure from the Danfoss sensor at the precombustion Chamber as a function of time



(d) The second pressure from the Danfoss sensor at the after-burn Chamber as a function of time

Figure 3.3: The Data from the four Danfoss sensors at different location on the Hybrid-rocket



(a) The pressure from the piezoelectric sensor at the H₂O₂ Chamber as a function of time

(b) The pressure from the piezoelectric sensor at the after-burn Chamber as a function of time

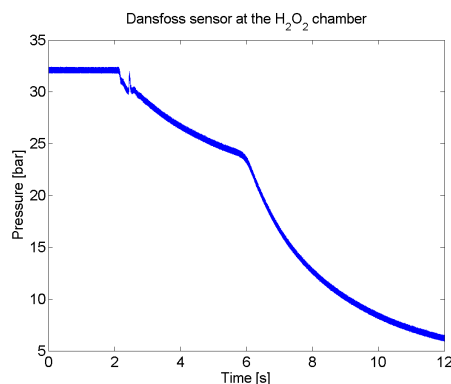
(c) The pressure from the piezoelectric sensor at the Precombustion Chamber as a function of time

(d) The pressure from the piezoresistive sensor at the after-burn Chamber as a function of time

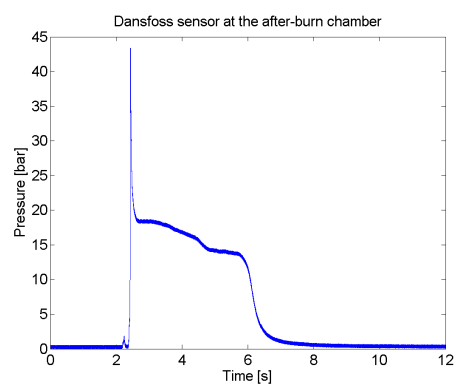
Figure 3.4: The Data from three piezoelectric and one piezoresistive sensor at different location on the Hybrid-rocket

3.1.4 Burn 4

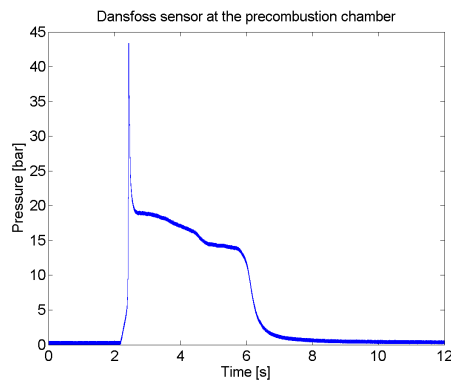
For the Third burn the engine functioned without any problems. However, the second Danfoss sensor at the precombustion chamber was not connected properly to the data acquisition system so the received data is only noise. The Pressure of the H₂O₂ chamber falls nicely linearly, and the data from the precombustion and after-burn chamber is similar in both the PE, PR and Danfoss sensors. The data from the PE-sensors have at the end of the run drifted a bit as can be seen by the slight raise it have from zero bar. What should be noticed in this burn is the especially high pressure peak in the precombustion and after-burn chamber, compared to the previous burns.



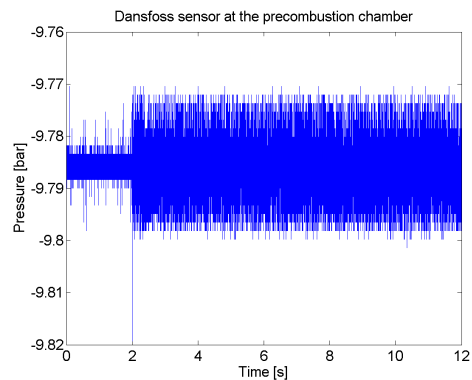
(a) The pressure from the Danfoss sensor at the H₂O₂ Chamber as a function of time



(b) The pressure from the Danfoss sensor at the after-burn Chamber as a function of time



(c) The first pressure from the Danfoss sensor at the precombustion Chamber as a function of time



(d) The second pressure from the Danfoss sensor at the precombustion Chamber as a function of time

Figure 3.5: The Data from the four Danfoss sensors at different location on the Hybrid-rocket

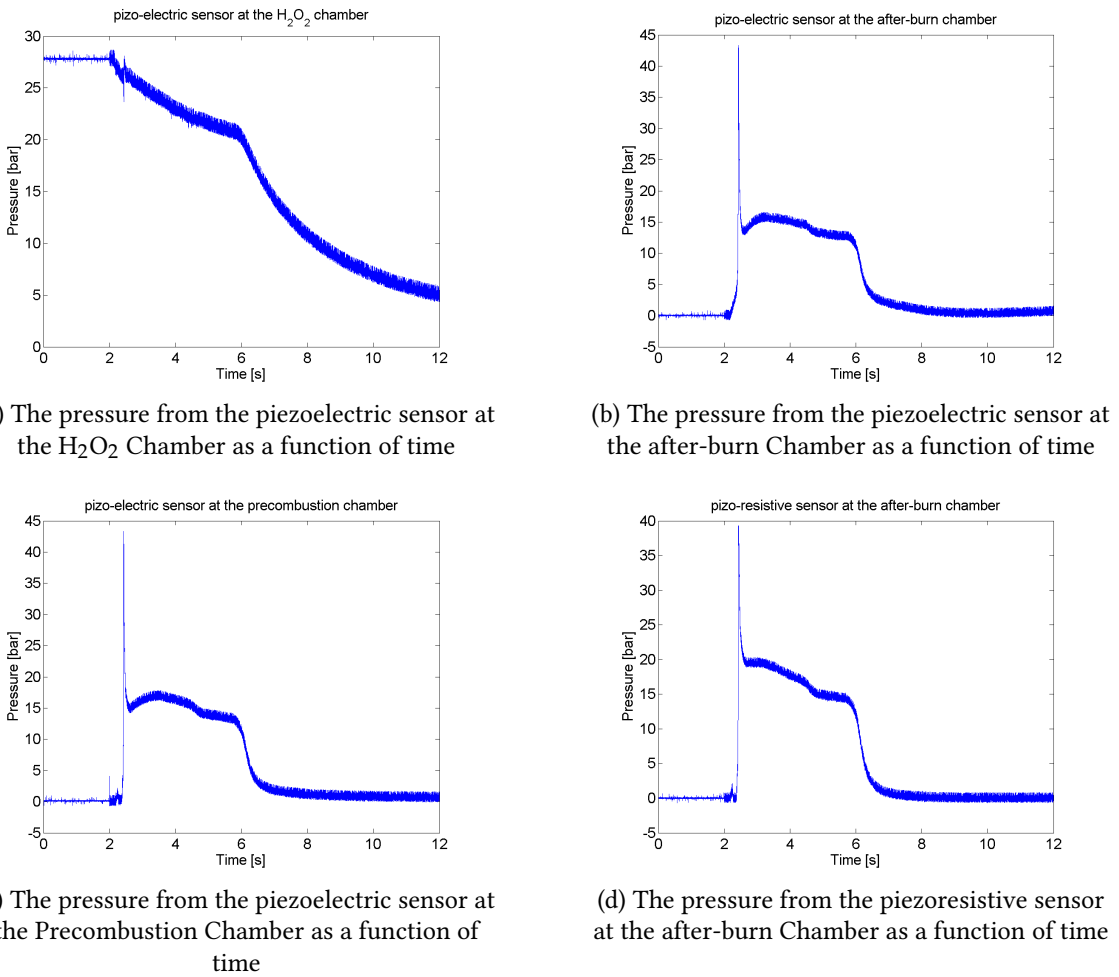


Figure 3.6: The Data from three piezoelectric and one piezo-resistive sensor at different location on the Hybrid-rocket

3.2 Methods of Analysis

3.2.1 Spectrum Analysis

To answer the questions stated, regarding the frequencies, a spectrum analysis of the signals has to be made. This is done with coding software MATLAB, applying Fast Fourier Transformation (FFT). FFT converts a signal in time-domain to a frequency domain. This is helpful to locate certain frequencies dominant to others.

3.2.2 Noise Isolation

Noise isolation is done first by making a moving average of the data to create a smooth function that describes the data.

The moving average is then subtracted from the data, this leaves only the noise behind.

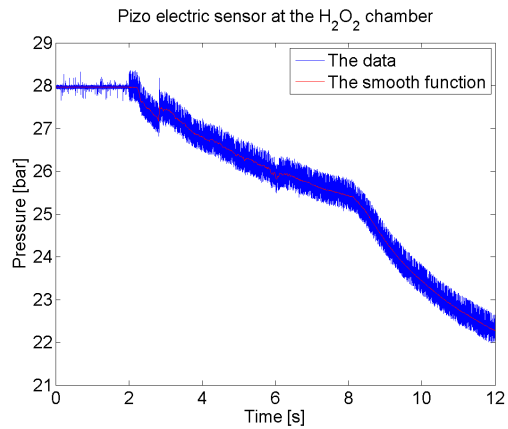


Figure 3.7: The data for the pressure as a function of time, with a moving average denotes as "The Smooth function"

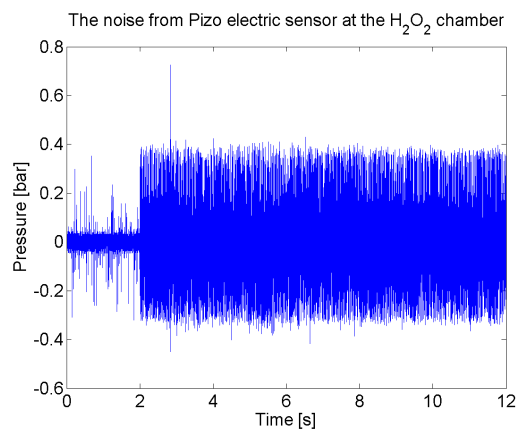


Figure 3.8: The noise for the pressure as a function of time, obtained through subtracting the moving average from the original data

The noise of different data sets can then be compared through different methods including Cross correlation.

3.2.3 Cross Correlation

Cross Correlation is defined through the equation

$$(f \star g)(\tau) \equiv \int_{-\infty}^{\infty} f^*(t)g(t + \tau)dt \quad (3.1)$$

where f^* denotes the complex conjugated of f . Cross correlation works by shifting the time scale of the function g and studying the changes in area. This way we can measure the similarities of $g(t)$ and $f(t)$ as a function of lag (τ) and use this information to get the time lag between the two. The discrete version of equation 3.1 is given by

$$(f \star g)(\tau) \equiv \sum_{m=-\infty}^{\infty} f^*(m)g(m + n) \quad (3.2)$$

3.3 Results

3.3.1 Physical measurements

The burn process can be seen in figure 3.9. Here the valve control, force and pressure from PR is shown as signals. They are not converted to physical quantities yet. The force signal is converted with the sensitivity of 100 N V^{-1} . The theoretical force calculated from chapter 1.4 is 824 N. This is around 8 V, which can be seen on the figure to be very likely. So the data fits the theory withing reasonable boundaries.

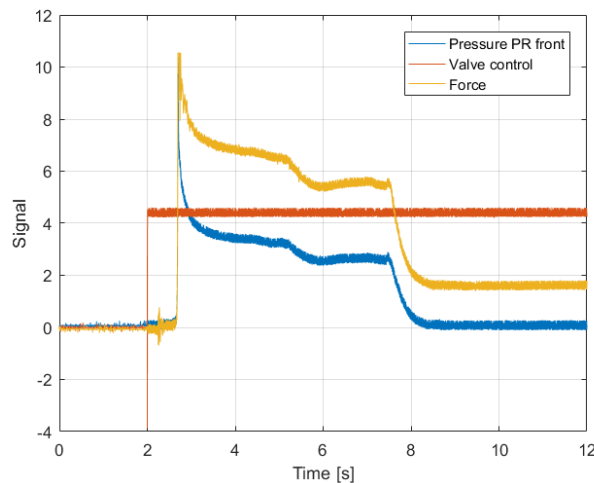


Figure 3.9: Raw signal of Burn 3

3.3.2 Frequency Analysis

The high frequency signal recorded from the piezoelectric, located in the afterburn chamber, is analysed in MATLAB by applying a fast Fourier transformation and reviewing the spectrum diagram. The pressure in the afterburn chamber has direct influence on the

force, and hence this is the interesting oscillations. The frequency analysis of this signal can be seen in figure 3.10. To emphasise the oscillation frequencies that are caused by the combustion only, the spectrum analysis from the pre-ignition signal is overlaid with a different color. This way, frequencies that are present at the combustion only, will stand out without a backup spike. The graph shows that there are no such frequencies from combustion only. All peaks from combustion are vague, and backed up by the background noise. They are assumed to originate from the electric noise and other background noise. The same applies for the signal from the other sensor, other location, and the other burns. So for this case, a sample rate as low as 100 Hz, would be sufficient in order to measure the pressure variations. Also, pressure fluctuations in hybrid rockets are known to exist at low frequencies, so a 10kHz sensor is not appropriate.

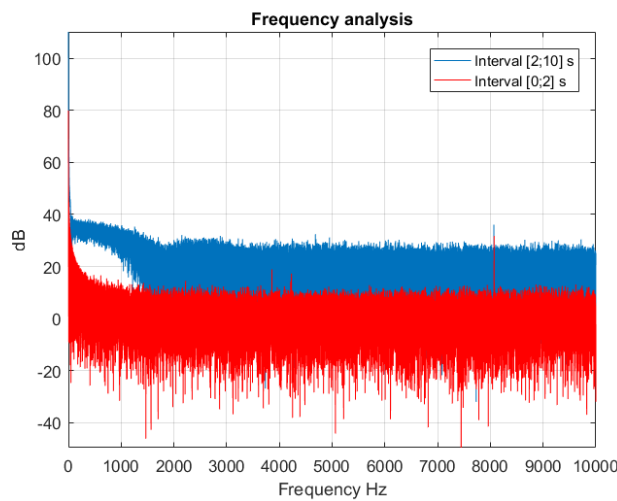


Figure 3.10: Frequency analysis of Burn 3, PR afterburn chamber, of burn time (blue) and pre-ignition only (red)

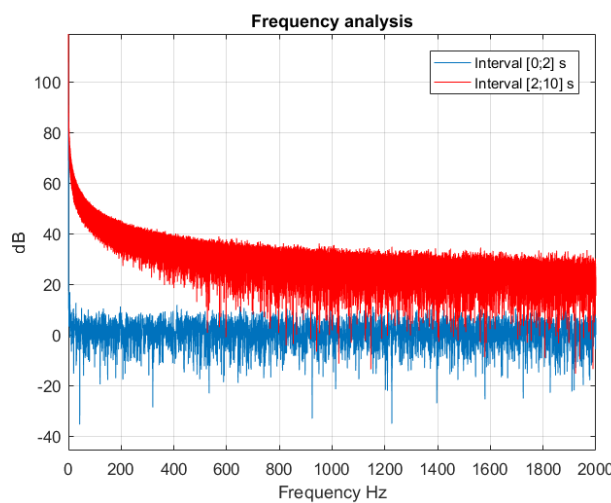


Figure 3.11: Frequency analysis of Burn 3, PE combustion chamber, of burn time (red) and pre-ignition only (blue)

To draw conclusions about the oscillations in the setup, another spectrum analysis is made in the force link of burn 1, at the lower frequency range. This is to determine any natural frequencies of the test rig itself. Figure 3.12 shows that there are some very vague distinguishable frequencies around 21, 35, 64 and 96 Hz. This knowledge can be used to exclude these frequencies, if searching for pressure oscillations in this spectrum.

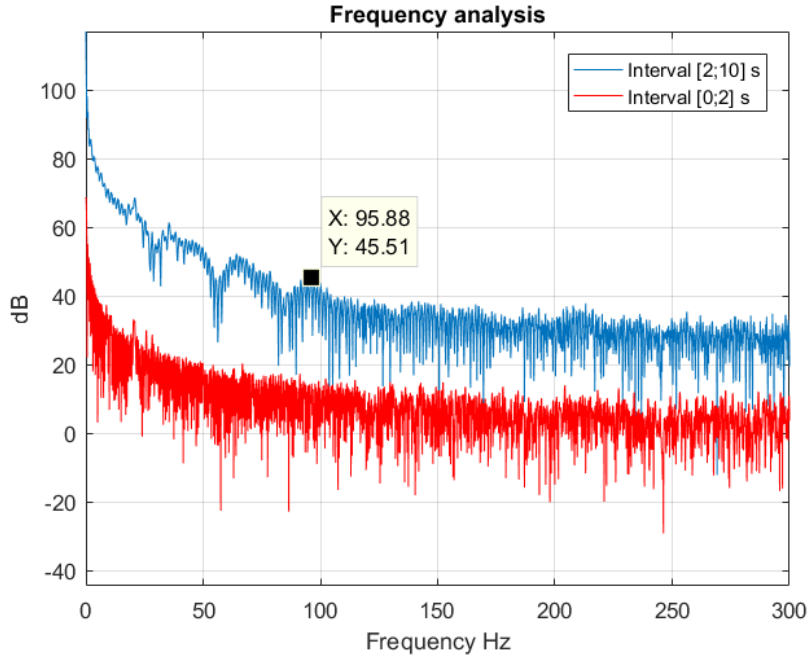


Figure 3.12: Frequency analysis of Burn 1 of burn time (blue) and pre-ignition only (red)

3.3.3 Time lag and it's relation to the temperature

We here uses cross-correlation to determined the lag between the measured pressure signal from the pre-combustion chamber to the after-burn chamber. The time it takes for the pressure to travel between the sensors is found through fist isolation the high-frequencies in each sensor (see subsection 3.2.2) and then compare these through cross-correlation (see subsection 3.2.3). As the lag between the sensors is equal to the speed of sound in the rocket and the speed of sound depends on the temperature (see equation 1.18). We choose only time intervals where the motor runs quit steady to insure that the lag is also approximately steady in the chosen time interval. To do calculations on the temperature from the speed of sound we rewrite equation 1.18

$$T = \frac{a^2}{\kappa R} \quad (3.3)$$

and because we only have the time of travel " t " between the sensors

$$a = L/t \quad (3.4)$$

$$\Rightarrow T = \frac{L^2}{\kappa R t^2} \quad (3.5)$$

where L is the distance between the sensors

The Danfoss Sensors

In this subsection we will compare the Danfoss sensors placed at different places throughout the rocket and calculate the time lag between them in order to find a average speed of sound aka the speed of the pressure wave through the rocket.

The value used in the calculation of equation 3.5 can be found in table 3.1 and the results in table 3.2

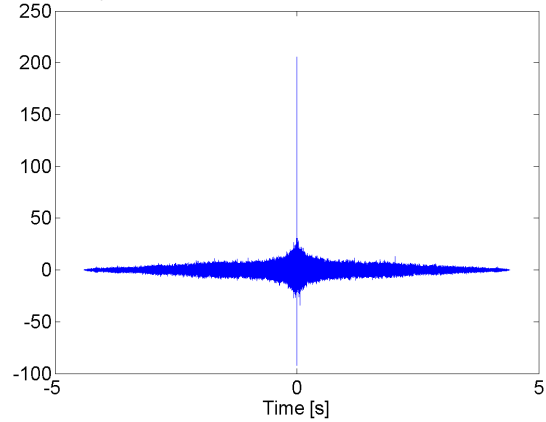
constant	value	unit
L	0.33	m
κ	1.2	
R	244.4373	$J/K\ kg$

Table 3.1: The values used in the calculation of equation 3.5

Burn nr.	Time interval [s]	t [s]	a [m/s]	T [K]
2	3.6-8.0	$1.4999 \cdot 10^{-4}$	$2.2001 \cdot 10^3$	$1.6502 \cdot 10^4$
3	3.5-4.6	$2.4999 \cdot 10^{-4}$	$1.3201 \cdot 10^3$	$5.9408 \cdot 10^3$
4	3.5-5.7	$2.4999 \cdot 10^{-4}$	$1.3201 \cdot 10^3$	$5.9408 \cdot 10^3$

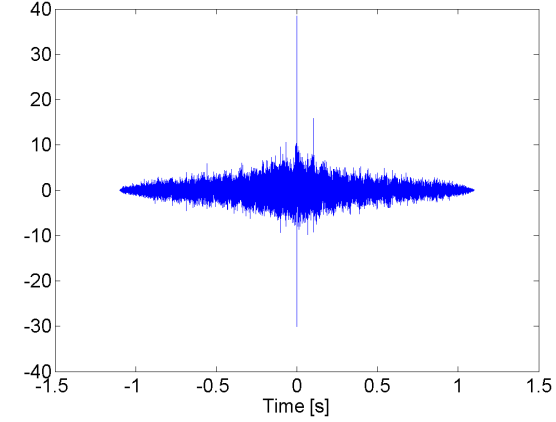
Table 3.2: The results of the cross-correlations between the Danfoss sensors, and the resulting speed and temperature

The Crosscorrelation of the noise between the two Danfoss sensors
at the precombustion and after-burn chambers from Burn 1



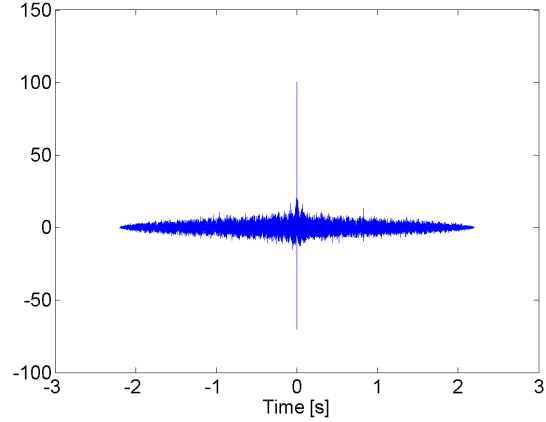
(a) Cross-correlation of noise between the precombustion
and the after-burn chamber from Burn 2

The Crosscorrelation of the noise between the two Danfoss sensors
at the precombustion and after-burn chambers from Burn 3



(b) Cross-correlation of noise between the precombustion
and the after-burn chamber from Burn 3

The Crosscorrelation of the noise between the two Danfoss sensors
at the precombustion and after-burn chambers from Burn 3



(c) Cross-correlation of noise between the precombustion
and the after-burn chamber from Burn 4

Figure 3.13: Cross-correlation of noise between the Danfoss sensors placed at the precombustion and the after-burn chamber from all Burns

The piezoelectric Sensors

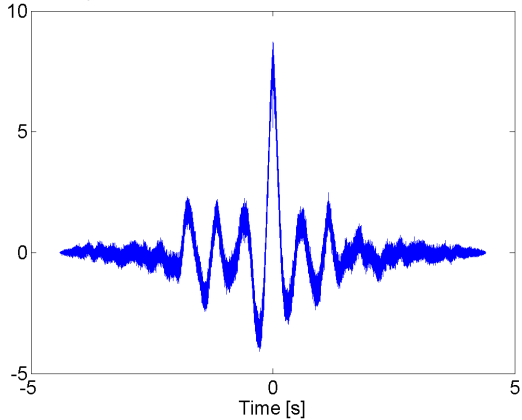
In this subsection we will compare the Danfoss sensors placed at different places throughout the rocket and calculate the time lag between them in order to find a average speed of sound aka the speed of the pressure wave through the rocket.

The value used in the calculation of equation 3.5 can be found in table 3.1 and the results in table 3.3.3

Burn nr.	Time interval [s]	t [s]	a [m/s]	T [K]
2	3.6-8.0	$4.0000 \cdot 10^{-4}$	825.00	$2.3204 \cdot 10^3$
3	3.5-4.6	$4.5000 \cdot 10^{-4}$	733.33	$1.8334 \cdot 10^3$
4	3.5-5.7	$3.0000 \cdot 10^{-4}$	1100.00	$4.1251 \cdot 10^3$

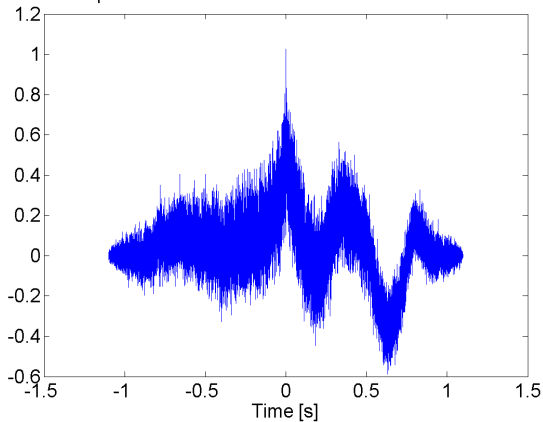
Table 3.3: The results of the cross-correlations between the piezoelectric sensors, and the resulting speed and temperature

The Crosscorrelation of the noise between the two pizo electric sensors
at the precombustion and after-burn chambers for Burn1



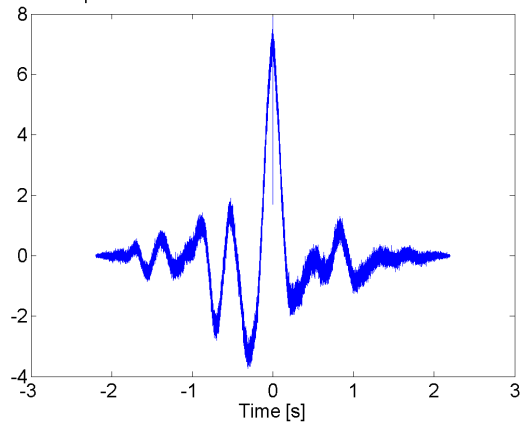
(a) Cross-correlation of noise between the precombustion
and the after-burn chamber from Burn 2

The Crosscorrelation of the noise between the two pizo electric sensors
at the precombustion and after-burn chambers for Burn 2



(b) Cross-correlation of noise between the precombustion
and the after-burn chamber from Burn 3

The Crosscorrelation of the noise between the two pizo electric sensors
at the precombustion and after-burn chambers for Burn 3



(c) Cross-correlation of noise between the precombustion
and the after-burn chamber from Burn 4

Figure 3.14: Cross-correlation of noise between the pizo electric sensors placed at the precombustion and the after-burn chamber from all Burns

Comparison

The results in table shows that we need a precision of the travel time to at least $1 \cdot 10^{-5}$ s to get a precise result. This criteria isn't fulfilled by the Danfoss sensors as can be seen in table 2.2, and is barely fulfilled by the piezoelectric sensor with their measurement frequency of 10kHz $\Rightarrow 1 \cdot 10^{-4}$ s precision. This is also the reason that the danfoss sensors give us something far away from the expected 2000K. Because of the short distance between the sensors the travel time also becomes very short, placing the sensors at greater distance from each other would therefore be preferable, to increase the precession.

3.3.4 Pressure Peak tracing

In this subsection we will use noise isolation followed by cross correlation on the two seconds of the data-set that includes the pressure peak (2 s to 4 s), to trace the pressure peak and its travel through the entire rocket. For comparison the exact time the data hit the top of the peaks will also be given as well as the time of travel this creates, this is a more rough estimate as it purely depends on the sensitivity of the sensors. the data analysis is done by following the procedure described in subsection 3.2.2 for the the sensors placed at the H₂O₂, precombustion and after-burn chamber, and now a cross-correlation of the ddata is done to find the lag (see table 3.5), aka the time that has the greatest positive correlation.

The Peaks is found simply by studying the local maxima's in the data (see table 3.4)).

The Data

In the following table's the notation is given in the following way

- FC symbolizes the H₂O₂ chamber.
- PC symbolizes the precombustion chamber.
- AB symbolizes the after-burn chamber.
- t_{i-j} is the difference in peak time, or the lag, between i and j . Where $i \wedge j =$ FC, PC, AB and $j \neq i$.

Burn nr.	Sensor Type	Peak 1 [s]	Peak 2 [s]	Peak 3 [s]	t_{FC-PC} peak [s]	t_{PC-AB} peak [s]	t_{FC-AB} peak [s]
2	Danfoss	2.7108	2.6967	2.6980	0.0141	0.0012	0.0128
3	Danfoss	2.4586	2.4306	2.4323	0.0279	0.0017	0.0262
1	PE	2.8410	2.8413	2.8336	0.0003	0.0077	0.0074
2	PE	2.7762	2.6977	2.7401	0.0785	0.0423	0.0361
3	PE	2.4597	2.4332	2.4301	0.0265	0.0030	0.0295

Table 3.4: The results form the peak to peak analysis

Burn nr.	Sensor Type	$t_{FC-PC \text{ cross}} [s]$	$t_{PC-AB \text{ cross}} [s]$	$t_{FC-AB \text{ cross}} [s]$
3	Danfoss	0.0104	0.00210	0.0086
4	Danfoss	0.0181	0.00140	0.0159
2	PE	0.0335	0.00045	0.0336
3	PE	0.0524	0.01560	0.0377
4	PE	0.0191	0.00200	0.0217

Table 3.5: The results from the cross-correlation in the time interval of 2 s to 4 s

Comparing the data

It comes as no shock that the burn that has the best correlation between the Danfoss sensor and PE sensors are Burn 4. As Burn 4 has the biggest pressure peak of the three data set. The first two data sets show only very little sign of the pressure peak in the H₂O₂ chamber which makes it hard to get an accurate correlation, and completely impossible for the Danfoss sensors in burn 2, which is why it has been omitted in table 3.4 and 3.5. A more detailed resolution of the sensor might help make the effects of the pressure peak more pronounced, if further study on this subject is done.

Chapter 4

Discussion and Conclusion

4.1 Discussion

The investigation was done with success since all estimations are within the expected range. By analyzing the measured data, it was found that the pressure and force were too stable in all burns to detect any distinguishable oscillations. To summarise:

- There are no distinguishable pressure oscillations in the afterburn- or combustion chamber.
- The Danfoss sensors of sample rate 250 Hz are sufficient enough to measure the low frequencies pressure variations. However, they are insufficient to measure the oscillations used to analyse wave speed propagation in the hybrid rocket.
- The wave speed was determined and used to calculate a combustion chamber temperature of approximately 2000 K.
- The Piezoelectric sensors are just sufficient to measure the wave speed propagation with their measurement frequency of 10 KHz $\Rightarrow 1 \cdot 10^{-4}$ s precision. However, a measurement precision of $1 \cdot 10^{-5}$ s would be desirable.
- If the effects of the pressure peak through out the rocket is desired to be studied in deeper detail, a better resolution of the pressure sensors placed on the H₂O₂ chamber is needed as to make the peak here more distinguishable.

4.2 Conclusion

All in all we think the project was successful. We got a proper understanding of the operation mode of a hybrid rocket and especially of the nozzle. During testing we could apply the gained knowledge successfully into practical application. Furthermore, we learned how to handle setbacks during project work and expanded our skill set in matters of academic research and writing as well as laboratory work.

Bibliography

- [1] Henrik Myhre Jensen. Note 0 - introduction to index notation and tensor analysis, 2015.
- [2] Alex Nørgaard, Anette Sø Kristensen, Martin Gosvig Jensen, and Anders Hjorth-Degenkolb Kristensen. UndersØgelse af regressionsrater i en hybrid raketmotor. Master's thesis, Aarhus University, 2015.
- [3] Cross-correlation. <https://en.wikipedia.org/wiki/Cross-correlation>, 2016. [Online; accessed 24-june-2016].
- [4] Oscar Biblarz and George P. Sutton. *Rocket Propulsion Elements*. Wiley-Interscience, 2001.
- [5] Danfoss A/S. Data sheet - pressure transmitters for industrial applications type mbs 32 and mbs 33, 2014.
- [6] Kistler Group. Data sheet - cylinder pressure sensor, 2013.
- [7] Kistler Group. Data sheet - piezoresistive pressure sensor, 2008.